Supplemental Information

Structural basis for Na^+-sensitivity in dopamine D2 and D3 receptors

Mayako Michino,[ab] R. Benjamin Free,[c] Trevor B. Doyle,[c] David R. Sibley[c] and Lei Shi*[abd]

SUPPLEMENTAL MATERIALS AND METHODS

Radioligand binding assays

Membrane binding assays were performed as previously described[1]. Briefly, HEK293 cells stably expressing either the human D_{2L} or D_3 dopamine receptors were grown in DMEM media (MediaTech/Cellgro, Manassas, VA) supplemented with 10% FBS, 50 U/ml penicillin, and 50 µg/ml streptomycin at 37°C in 5% CO2 and 90% humidity. Cells were harvested and then disrupted using dounce homogenization in 5 mM Tris-HCl, 7.4 at 4°C, and 5 mM $MgCl_2$. Cell lysate was divided into two equal aliquots and then centrifuged at 34,000 x g for 30 min. Membrane pellets were then re-suspended in either 50 mM Tris-HCl, pH 7.4 at 25°C (Na^+ *minus* buffer) or Earle's Balanced Salt Solution (EBSS - Na^+ *plus* buffer) (US Biological, San Antonio, TX). The EBSS buffer contains a Na^+ concentration of 144 mM. Similar results were obtained by adding Na^+ salts to the Tris-HCl buffer at a final concentration of 140-150 mM (data not shown). The membranes were incubated for 90 min at room temperature with 0.5 nM of [^{3}H]-N-methylspiperone (Perkin Elmer, Waltham, MA) and various concentrations of competing ligand. Bound ligand was separated from free by filtration through a PerkinElmer Unifilter-96 GF/C 96 well micro-plate using the PerkinElmer Unifilter-96 Harvester. After drying, 50 µL of liquid scintillation cocktail (MicroScint PS, Perkin Elmer, Waltham, MA) was added to each well, plates were sealed, and analyzed on a PerkinElmer Topcount NXT^{TM}. Data were normalized as a percentage of the control specific radioligand binding observed in the absence of competing ligand. For competition assays, K_i values were calculated from observed IC_{50} values using the Cheng-Prusoff equation[2].

Molecular docking

The ligands were docked to equilibrated models of D3R and D2R, which are based on the D3R crystal structure[3]. Docking was performed using induced-fit docking protocol in the Schrödinger software (release 2013-3; Schrödinger, LLC: New York, NY). The best-scoring pose that is consistent with the crystallographic ligand conformation and known experimental receptor-ligand interactions was selected. For sulpiride, a pose similar to that of eticlopride in the D3R crystal structure was selected, with the tertiary amine in the ethyl-pyrrolidine moiety forming a salt bridge to the Asp(3.32) side chain, and the methoxy-substituent of the benzamide moiety forming an intramolecular hydrogen bond with the amide-NH. For

spiperone, a pose with the butyrophenone moiety in the orthosteric binding site (OBS) was selected, in which π-π interactions are formed with aromatic residues in TM6, in agreement with site-directed mutagenesis data, and structure-activity relationship data of spiperone and its analogs[4] – modifications of the spiro-moiety such as in N-methylspiperone and NAPS result in small changes in affinity[4c], whereas modifications in the aliphatic portion of butyrophenone results in large changes over 10-fold in affinity[4a], suggesting that the butyrophenone moiety likely binds in the OBS. For zotepine, the pose in which the tricyclic moiety is bound in the OBS was selected, with the conformation of the tricyclic moiety similar to the crystallographic conformation of the compound[5].

Molecular dynamics (MD) simulations

MD simulations of the receptor-ligand complexes were performed in the explicit water-POPC lipid bilayer solvent environment using NAMD[6] (version 2.9). The position of Na^+ bound at the negatively charged Asp(2.50) was acquired by superimposing the Na^+-bound structure of adenosine A_{2A} receptor[7] to our D3R and D2R models. The system charges were neutralized by Cl^- ions for the condition in the absence of Na^+, Na^+ and Cl^- ions corresponding to a concentration of 0.15 M NaCl were added for the condition in the presence of Na^+. The total system consisted of ~77000 atoms. The CHARMM27 parameters with CMAP correction terms[8] were used for the protein, CHARMM36 parameters for the lipids[9], and TIP3P model for the water. The ligand parameters were obtained from the GAAMP server[10], with the initial force field based on CGenFF with ParamChem[11]. The protonation states of the ligands at pH 7.0 were predicted by the Epik program in the Schrödinger software (release 2013-3, Schrödinger, LLC: New York, NY, 2013). In the simulations, periodic boundary conditions were applied, a cutoff distance of 12 Å was used for the nonbonded interactions, and the particle-mesh Ewald summation method was used for the electrostatics interactions. The integration timestep was set to 2 fs, with the pairlists updated every 10 timesteps, the nonbonded forces calculated every timestep, and the full electrostatics forces calculated every two timesteps. Constant temperature (310 K) was maintained with Langevin dynamics, and 1 atm constant pressure was achieved by using the hybrid Nosé-Hoover Langevin piston method on a flexible periodic cell, with a constant-ratio constraint applied on the lipid bilayer in the X-Y plane. The system was initially minimized for 6000 steps and equilibrated with restraints on the heavy atoms of protein and ligand and bound Na^+ in the beginning (1 ns), then with restraints only on the Cα atoms of protein for 1 ns. The production stage was carried out with all atoms unrestrained.

Ligand binding energy calculations

The MM/GBSA ligand-receptor binding energy was calculated using CHARMM[12] (version c36a2) with the GBSW implicit solvent model[13]. For each frame being considered, the protein and ligand components

were extracted, then minimized with restraints on all heavy atoms except for the side chains within 4 Å of the ligand, before the energies were calculated.

Interaction network analysis

The pairwise residue interactions were computed and compared using a previously developed interaction network analysis protocol[14]. Briefly, two residues are defined to be in contact if either the distance between any two heavy atoms from the two residues is smaller than the sum of their van der Waals radii plus 0.6 Å[15], or polar interactions exist between the two residues as calculated by the HBPLUS program. The frames of MD trajectories at 240 ps interval were used for the analysis. All frames were clustered by Cα RMSD, then for each ligand, the frequencies of pairwise residue interactions were compared between the clusters representing the Na^+-bound and -unbound conditions. Significant difference in the pairwise residue interaction frequencies between the conditions was detected if the absolute log frequency ratio (log $frequency_1/frequency_2$) was above 0.8, and at least one of the frequencies was above 0.3.

Principal component analysis

The principal component analysis was performed using the Gromacs[16] programs *g_covar* and *g_anaeig*. The computed primary motion is shown in Fig. 4B as linear interpolations between negative and positive extremes of deformations along the first principal mode of motion.

SUPPLEMENTAL DISCUSSION

In addition to the effect on ligand binding affinity, Na^+-binding has also been implicated in modulating signaling efficacy. The comparison of the Na^+-bound inactive-state structure to the active-state A_{2A} adenosine receptor structure showed the Na^+/water pocket in the active state collapses in volume from ~200 to 70 $Å^3$ due to movements of TM helices and would not allow coordination for Na^+ [7, 17]. The collapse of the Na^+-binding site is thus suggested to correlate with the unbinding of Na^+ and contribute to the negative allosteric effect of Na^+ on agonist-binding[18]. Furthermore, Ala mutations of residues Asp(2.50), Asn(7.49), Ser(3.39), Trp(6.48), and Asn(7.45) were shown to either abrogate or reduce the agonist-stimulated receptor signaling[19]. In addition, Na^+ dissociation in the active state may shift the protonation state of Asp(2.50), and be related to the pH-dependence of activation in β2AR[20]. In this paper, however, we characterize an Na^+-unbound inactive state that is yet to be revealed by crystallography – in contrast to all the crystal structures of aminergic receptors[21], the Asp(3.32)-Tyr(7.43) interaction is dissociated in this state, which can be stabilized by a bulky Na^+-insensitive ligand like spiperone.

Table S1. List of MD simulations. Multiple MD trajectories were collected for each receptor-ligand complex in the Na^+-bound and -unbound conditions.

Receptor	Ligand	Na+	Number of trajectories	Simulation lengths
D3R	eticlopride	+	2	600, 300
		-	2	600, 300
	sulpiride	+	3	300, 300, 300
		-	3	300, 300, 450
	spiperone	+	2	300, 400
		-	1	400
D2R	eticlopride	+	3	120, 120, 120
	sulpiride	+	2	300, 300
		-	2	400, 600
	spiperone	+	1	300
	zotepine	+	1	300
		-	2	180, 360
	zotepine-analog	+	1	180
		-	1	180

Fig. S1. Chemical structures of the Na^+-sensitive and insensitive ligands used in this study.

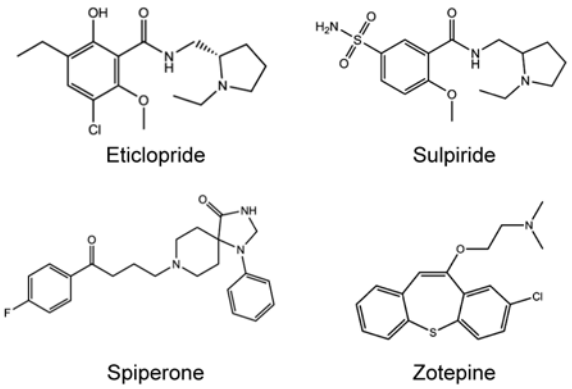

Fig. S2. Experimental binding affinity curves for the D3R with and without Na^+ for sulpiride, eticlopride, spiperone, and zotepine. Radioligand binding assays with D3R containing membranes were performed as described in the Methods section. Membranes were incubated with 0.5 nM [^{3}H]-methylspiperone and the indicated concentrations of competing ligand in the absence or presence of 144 mM Na^+. The data are expressed as a percentage of the control [^{3}H]-methylspiperone binding observed in the absence of competing ligand. The curves displayed represent an average of three independent experiments. K_i values were calculated from the IC_{50} values using the Cheng-Prusoff equation[2] and are as follows: eticlopride: 0.170 ± 0.02 nM (-Na^+), 0.074 ± 0.03 nM (+Na^+); sulpiride: 622 ± 6.9 nM (-Na^+), 15.2 ± 3.1 nM (+Na^+); spiperone: 1.03 ± 0.18 nM (-Na+), 1.63 ± 0.29 nM (+Na^+); zotepine: 16.3 ± 0.69 nM (-Na^+), 59 ± 12.4 nM (+Na^+).

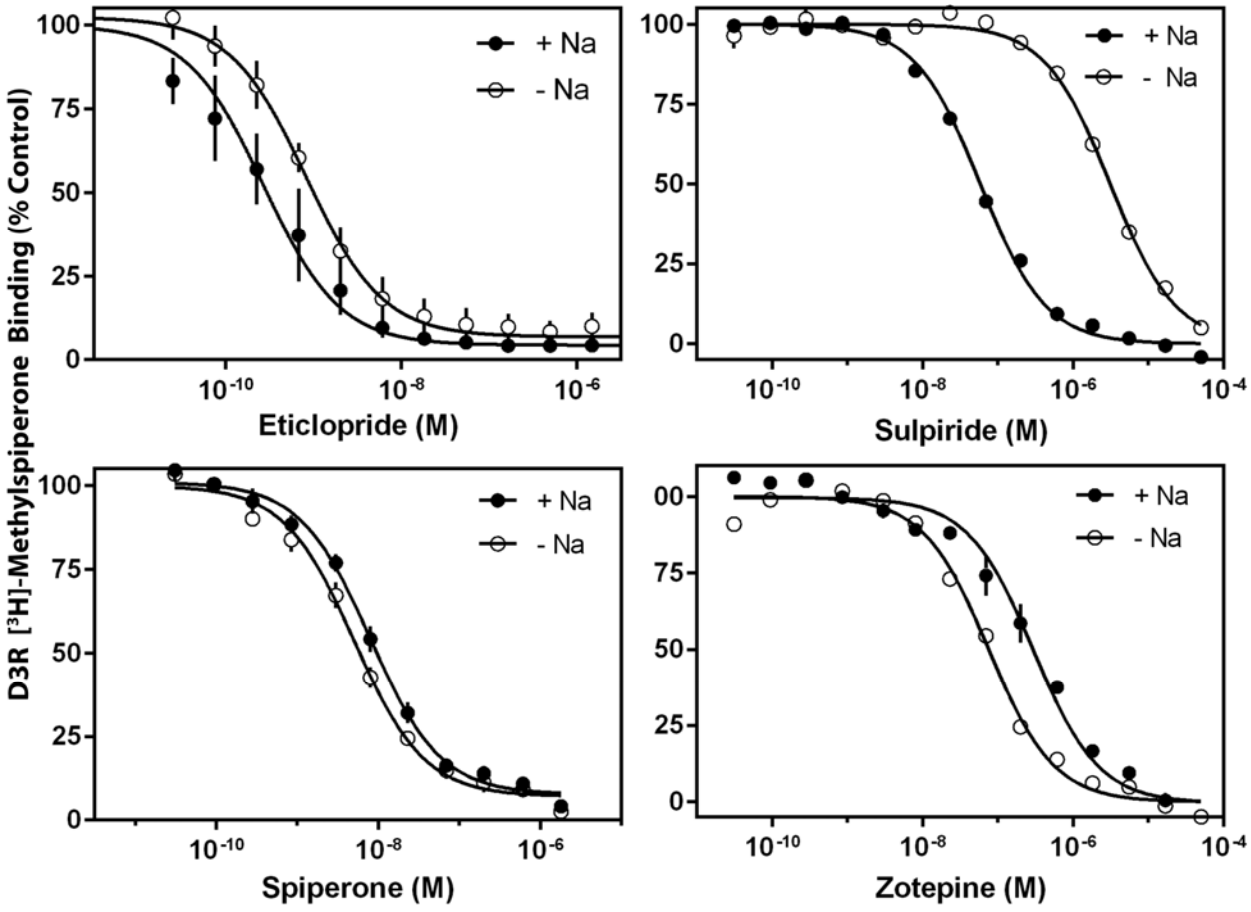

Fig. S3. Structural characterization of the Na^+-binding site residues. The distribution of distance between the Na^+ and nearby oxygen atoms for residues at the Na^+-binding site in the eticlopride (A), sulpiride (B), spiperone (C), and zotepine (D) simulations. (E) The frequencies of the frames with the indicated numbers of water within 3.0 Å of Na^+.

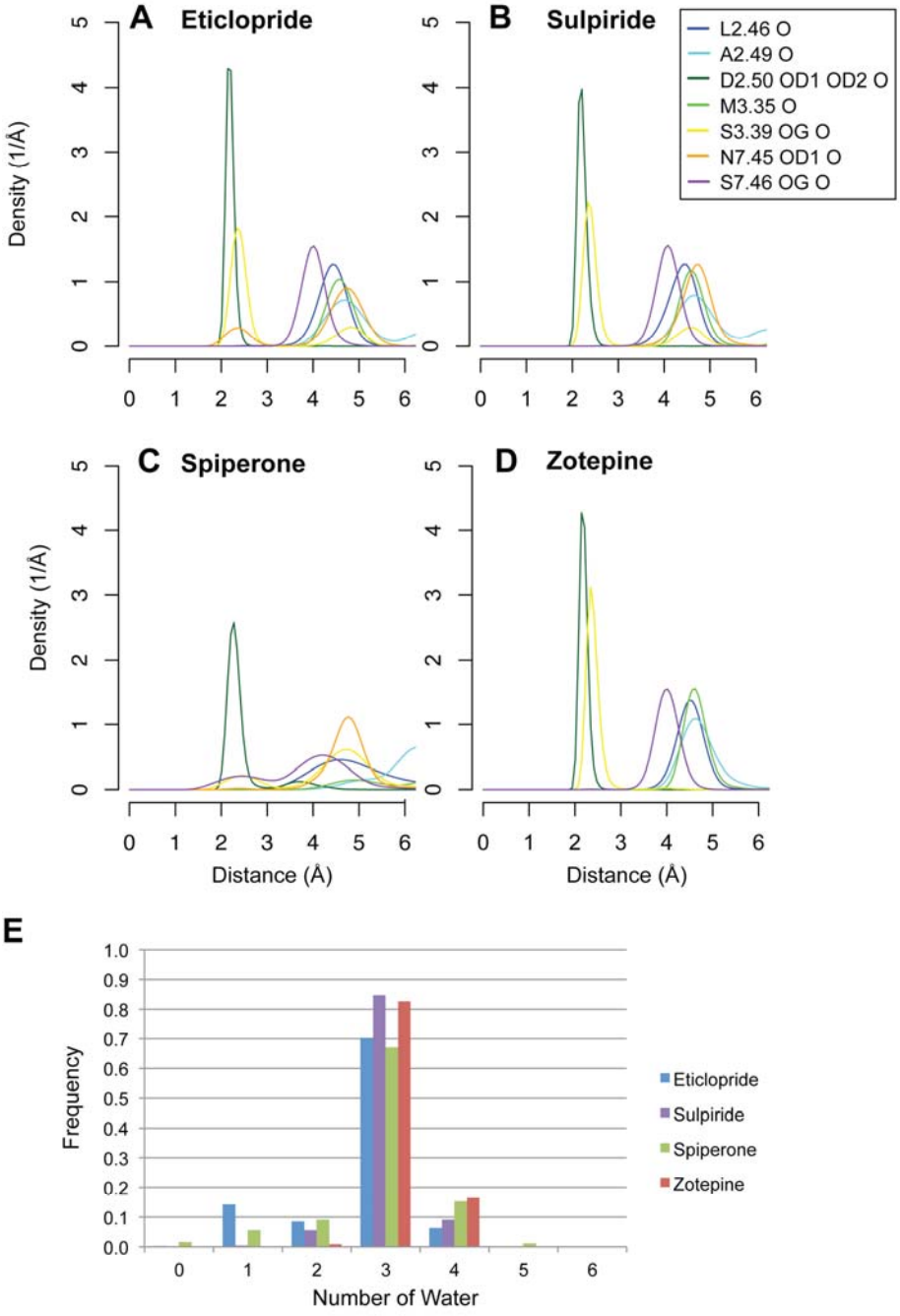

Fig. S4. Preferred conformations of zotepine and its analog without the ethoxy oxygen atom. (A) Structures of zotepine (cyan) and its analog with the ethoxy O atom replaced by a C atom (orange). The distance between the N3 and O6 atoms in zotepine (N4 and C3 atoms in the analog) is indicated as a black dotted line. The N3-C1-C2-O6 dihedral angle in zotepine (N4-C1-C2-C3 in the analog) is indicated as a black arrow. (B) Conformational search of zotepine and its analog was performed using MacroModel (version 2014-3, Schrödinger, Inc., New York, NY). The resulting conformers were clustered by the distance and dihedral angle shown in (A). The clusters of lowest energy conformers are indicated by black arrows. Zotepine has two clusters of lowest-energy conformers with the N3-O6 distance of ~2.8 Å and the N3-C1-C2-O6 dihedral angle of ~-60 or -300 degrees, whereas the analog has one lowest-energy cluster with the N4-C3 distance of ~3.9 Å and the N4-C1-C2-C3 dihedral angle of ~-180 degrees.

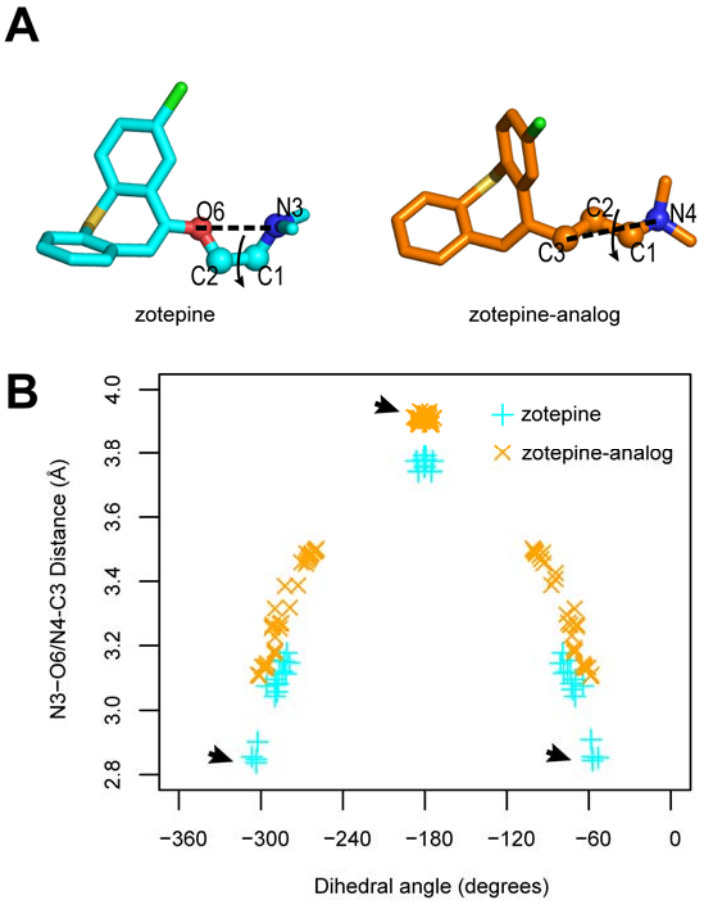

Fig. S5. MD simulations of D2R in complex with zotepine and its analog without the ethoxy oxygen atom. The binding modes of zotepine (A) and its analog (B) in the Na^+-bound (green) and –unbound (gray) simulations. (C) The distance between Asp(3.32) Oδ and protonated N atom of ligand for zotepine and its analog. The red dotted line shows the corresponding distance in the D3R-eticlopride crystal structure[3] (2.7 Å). (D) The intramolecular distance between the N3 and O6 atoms (N4 and C3 atoms in the analog). For panels (C) and (D), each bar represents the average value for the particular configuration, and the error bar indicates the standard deviation. (E) Distributions of the N3-C1-C2-O6 dihedral angle in the zotepine (N4-C1-C2-C3 dihedral angle in the analog) simulations. In the absence of Na^+, the salt bridge between the protonated N of the ligand and Asp(3.32) Oδ breaks, and the intramolecular N3-O6 interaction is shortened for zotepine, but not for the analog. See Fig. S4 (A) for definitions of the distances and dihedral angles.

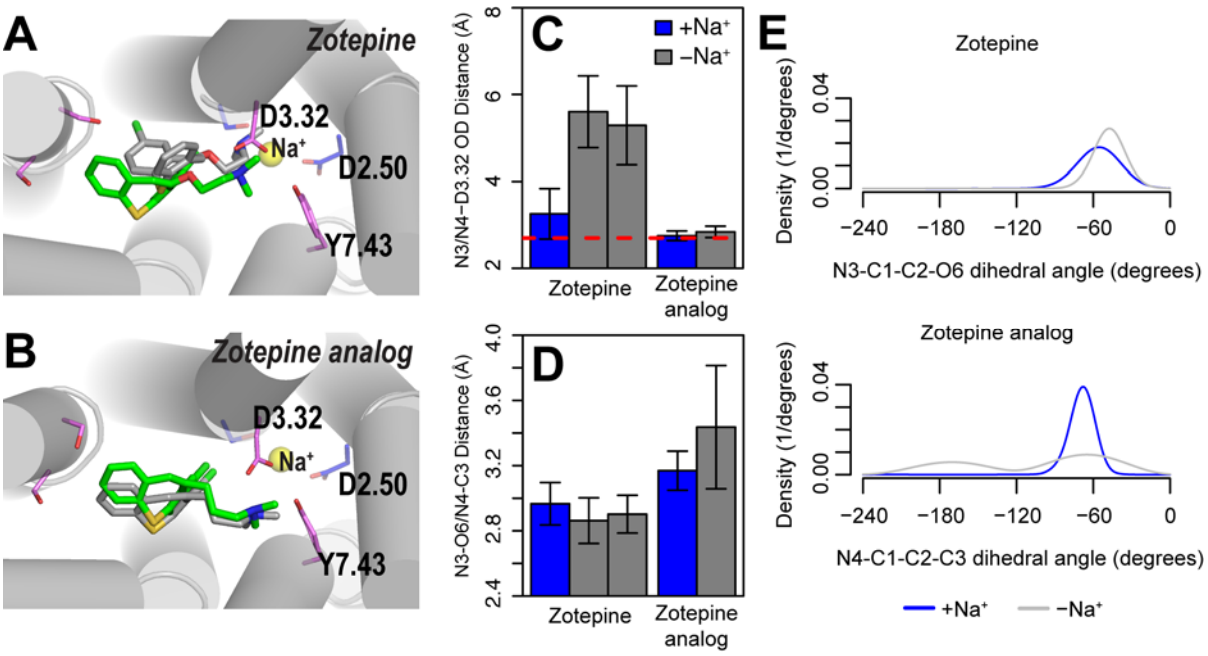

Fig. S6. Comparison of the distributions of the Ser(3.39) χ1 dihedral angle in the Na^+-bound and –unbound conditions for the eticlopride, sulpiride, spiperone, and zotepine simulations.

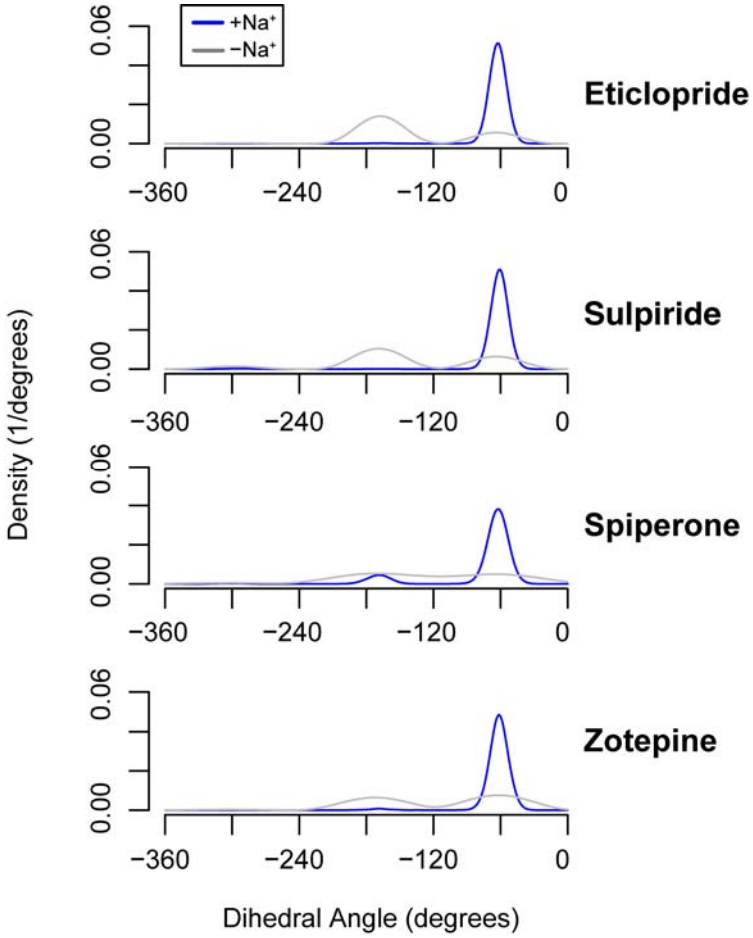

Fig. S7. Structural characterization of the receptor conformations outside of the Na^+-binding site. Comparison of the Asp(3.32) Oδ -Tyr(7.43) OH distance (A), and Cys(3.36) Cβ -Phe(6.44) Cβ distance (B) in the Na^+-bound and -unbound conditions. Each bar represents the average value for the particular condition, and the error bar indicates the standard deviation. The red dotted line shows the corresponding distance in the D3R-eticlopride crystal structure[3] (2.7 Å (A), 9.7 Å (B)); the orange dotted lines show the distances in the β_2-adrenergic receptor inactive[22] (thick dotted: 2.7 Å (A), 9.4 Å (B)) and active[23] (thin-dotted: 2.5 Å (A), 12.1 Å (B))-state structures.

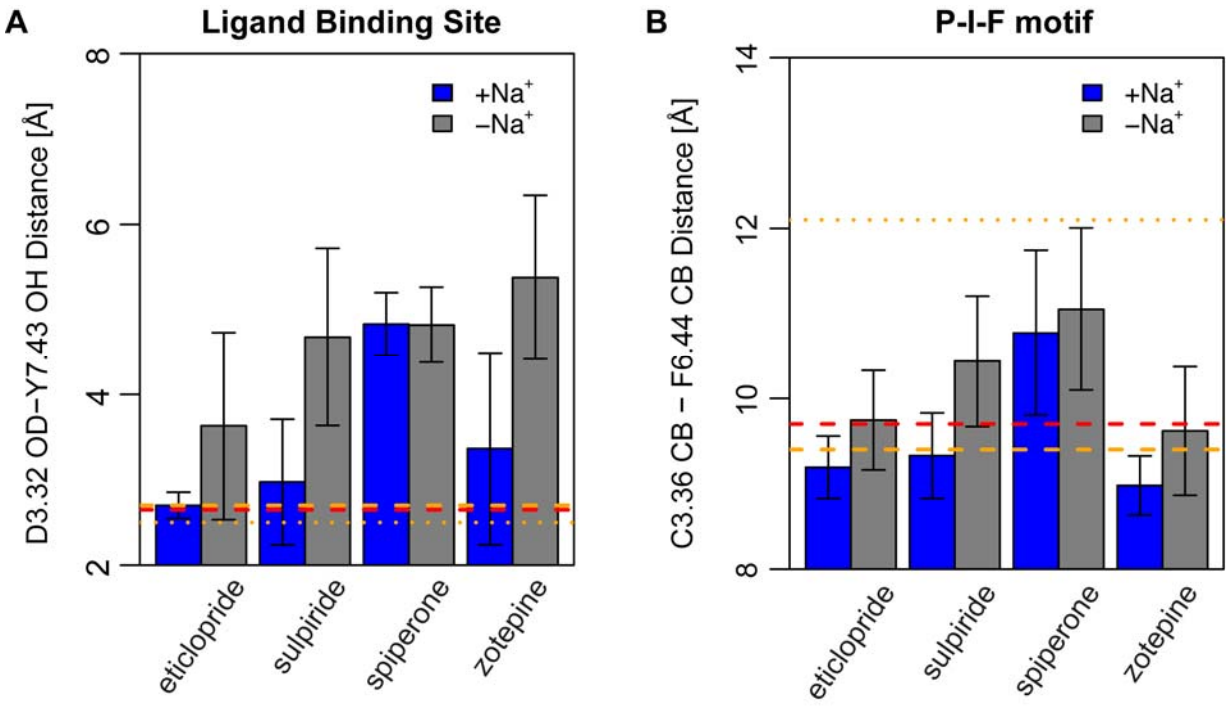

Fig. S8. Ligand and receptor stability in the MD simulations of D3R-eticlopride and D3R-sulpiride. (A) Comparison of the distributions of ligand dihedral angle between the amide and benzene moieties of eticlopride and sulpiride (the O8-C1-C2-O7 dihedral angles are indicated by black arrows in the inset ligand structures) in the D3R-eticlopride and D3R-sulpiride simulations shows a narrower distribution for eticlopride. The distributions from the Na^+-bound simulations are in solid lines, and those from the Na^+-unbound simulations are in dotted lines. (B) The stability of the Asp(3.32) Oδ -Tyr(7.43) OH interaction in the Na^+-unbound simulations of D3R-eticlopride and D3R-sulpiride is represented as barplots. Each bar corresponds to a single simulation trajectory. The dark gray and light gray areas indicate the segments of the simulations for which the interaction is maintained.

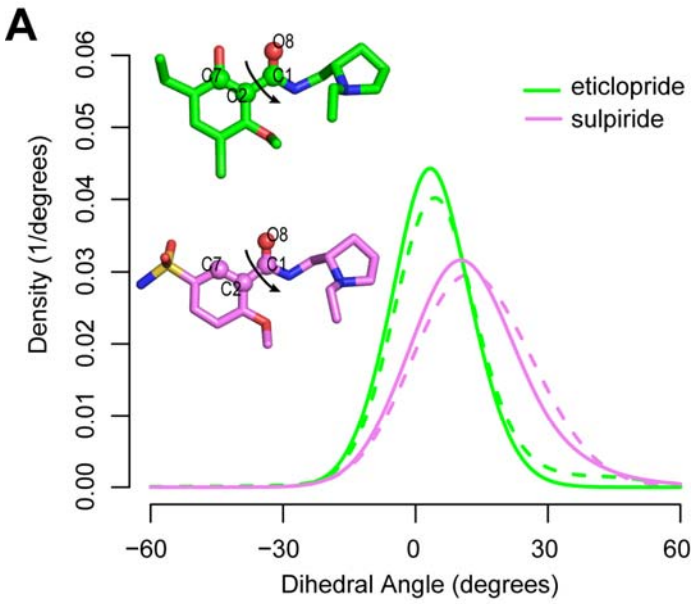

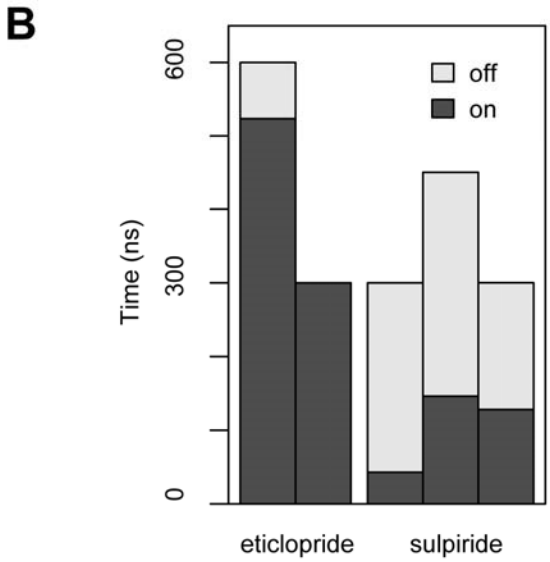

REFERENCES

1(a) L. S. Chun, R. B. Free, T. B. Doyle, X. P. Huang, M. L. Rankin and D. R. Sibley, *Molecular pharmacology*, 2013, **84**, 190; (b) R. B. Free, L. S. Chun, A. E. Moritz, B. Miller, T. B. Doyle, J. L. Conroy, A. Padron, J. A. Meade, J. Xiao, X. Hu, A. E. Dulcey, Y. Han, L. Duan, S. Titus, M. Bryant-Genevier, E. Barnaeva, M. Ferrer, J. A. Javitch, T. Beuming, L. Shi, N. Southall, J. J. Marugan and D. R. Sibley, *Molecular pharmacology*, 2014.

2 Y. Cheng and W. H. Prusoff, *Biochemical pharmacology*, 1973, **22**, 3099.

3 E. Y. Chien, W. Liu, Q. Zhao, V. Katritch, G. W. Han, M. A. Hanson, L. Shi, A. H. Newman, J. A. Javitch, V. Cherezov and R. C. Stevens, *Science*, 2010, **330**, 1091.

4(a) D. O. Kiesewetter, W. C. Eckelman, R. M. Cohen, R. D. Finn and S. M. Larson, *International journal of radiation applications and instrumentation. Part A, Applied radiation and isotopes*, 1986, **37**, 1181; (b) F. Boeckler, H. Lanig and P. Gmeiner, *J Med Chem*, 2005, **48**, 694; (c) L. Albizu, M. Cottet, M. Kralikova, S. Stoev, R. Seyer, I. Brabet, T. Roux, H. Bazin, E. Bourrier, L. Lamarque, C. Breton, M. L. Rives, A. Newman, J. Javitch, E. Trinquet, M. Manning, J. P. Pin, B. Mouillac and T. Durroux, *Nature chemical biology*, 2010, **6**, 587.

5 I. Kalofonos, D. Kalofonos, W. Martin-Doyle, J. Hanko and E. J. Hagen, Google Patents, 2011.

6 J. C. Phillips, R. Braun, W. Wang, J. Gumbart, E. Tajkhorshid, E. Villa, C. Chipot, R. D. Skeel, L. Kale and K. Schulten, *Journal of computational chemistry*, 2005, **26**, 1781.

7 W. Liu, E. Chun, A. A. Thompson, P. Chubukov, F. Xu, V. Katritch, G. W. Han, C. B. Roth, L. H. Heitman, A. P. Ijzerman, V. Cherezov and R. C. Stevens, *Science*, 2012, **337**, 232.

8(a) A. D. MacKerell, D. Bashford, M. Bellott, R. L. Dunbrack, J. D. Evanseck, M. J. Field, S. Fischer, J. Gao, H. Guo, S. Ha, D. Joseph-McCarthy, L. Kuchnir, K. Kuczera, F. T. Lau, C. Mattos, S. Michnick, T. Ngo, D. T. Nguyen, B. Prodhom, W. E. Reiher, B. Roux, M. Schlenkrich, J. C. Smith, R. Stote, J. Straub, M. Watanabe, J. Wiorkiewicz-Kuczera, D. Yin and M. Karplus, *The journal of physical chemistry. B*, 1998, **102**, 3586; (b) A. D. Mackerell, Jr., M. Feig and C. L. Brooks, 3rd, *Journal of computational chemistry*, 2004, **25**, 1400.

9 J. B. Klauda, R. M. Venable, J. A. Freites, J. W. O'Connor, D. J. Tobias, C. Mondragon-Ramirez, I. Vorobyov, A. D. MacKerell, Jr. and R. W. Pastor, *The journal of physical chemistry. B*, 2010, **114**, 7830.

10 L. Huang and B. Roux, *Journal of chemical theory and computation*, 2013, **9**.

11 K. Vanommeslaeghe, E. Hatcher, C. Acharya, S. Kundu, S. Zhong, J. Shim, E. Darian, O. Guvench, P. Lopes, I. Vorobyov and A. D. Mackerell, Jr., *Journal of computational chemistry*, 2010, **31**, 671.

12 B. R. Brooks, C. L. Brooks, 3rd, A. D. Mackerell, Jr., L. Nilsson, R. J. Petrella, B. Roux, Y. Won, G. Archontis, C. Bartels, S. Boresch, A. Caflisch, L. Caves, Q. Cui, A. R. Dinner, M. Feig, S. Fischer, J. Gao, M. Hodoscek, W. Im, K. Kuczera, T. Lazaridis, J. Ma, V. Ovchinnikov, E. Paci, R. W. Pastor, C. B. Post, J. Z. Pu, M. Schaefer, B. Tidor, R. M. Venable, H. L. Woodcock, X. Wu, W. Yang, D. M. York and M. Karplus, *Journal of computational chemistry*, 2009, **30**, 1545.

13 W. Im, M. S. Lee and C. L. Brooks, 3rd, *Journal of computational chemistry*, 2003, **24**, 1691.

14 S. Stolzenberg, M. Quick, C. Zhao, K. Gotfryd, G. Khelashvili, U. Gether, C. J. Loland, J. A. Javitch, S. Noskov, H. Weinstein and L. Shi, *J Biol Chem*, in press.

15 A. J. Venkatakrishnan, X. Deupi, G. Lebon, C. G. Tate, G. F. Schertler and M. M. Babu, *Nature*, 2013, **494**, 185.

16 S. Pronk, S. Pall, R. Schulz, P. Larsson, P. Bjelkmar, R. Apostolov, M. R. Shirts, J. C. Smith, P. M. Kasson, D. van der Spoel, B. Hess and E. Lindahl, *Bioinformatics*, 2013, **29**, 845.

17 V. Katritch, V. Cherezov and R. C. Stevens, *Annual review of pharmacology and toxicology*, 2013, **53**, 531.

18 H. Gutierrez-de-Teran, A. Massink, D. Rodriguez, W. Liu, G. W. Han, J. S. Joseph, I. Katritch, L. H. Heitman, L. Xia, A. P. Ijzerman, V. Cherezov, V. Katritch and R. C. Stevens, *Structure*, 2013, **21**, 2175.

19 A. Massink, H. Gutierrez-de-Teran, E. B. Lenselink, N. V. Ortiz Zacarias, L. Xia, L. H. Heitman, V. Katritch, R. C. Stevens and A. P. Ijzerman, *Molecular pharmacology*, 2015, **87**, 305.

20(a) A. Ranganathan, R. O. Dror and J. Carlsson, *Biochemistry*, 2014, **53**, 7283; (b) P. Ghanouni, H. Schambye, R. Seifert, T. W. Lee, S. G. Rasmussen, U. Gether and B. K. Kobilka, *J Biol Chem*, 2000, **275**, 3121.

21 M. Michino, T. Beuming, P. Donthamsetti, A. H. Newman, J. A. Javitch and L. Shi, *Pharmacol Rev*, 2015, **67**, 198.

22 V. Cherezov, D. M. Rosenbaum, M. A. Hanson, S. G. Rasmussen, F. S. Thian, T. S. Kobilka, H. J. Choi, P. Kuhn, W. I. Weis, B. K. Kobilka and R. C. Stevens, *Science*, 2007, **318**, 1258.

23 A. M. Ring, A. Manglik, A. C. Kruse, M. D. Enos, W. I. Weis, K. C. Garcia and B. K. Kobilka, *Nature*, 2013, **502**, 575.